Biosynthesis of ZnO nanoparticles using Jacaranda mimosifolia flowers extract: Synergistic antibacterial activity and...

Article *in* Journal of Photochemistry and Photobiology B Biology · June 2016

DOI: 10.1016/j.jphotobiol.2016.06.043

CITATIONS
2

READS
186

7 authors, including:

Deepali Sharma
University of KwaZulu-Natal
18 PUBLICATIONS **142** CITATIONS
SEE PROFILE

Gulshan Singh
Durban University of Technology
29 PUBLICATIONS **156** CITATIONS
SEE PROFILE

Thor Axel Stenström
Durban University of Technology
151 PUBLICATIONS **3,075** CITATIONS
SEE PROFILE

Krishna Bisetty
Durban University of Technology
98 PUBLICATIONS **553** CITATIONS
SEE PROFILE

Journal of Photochemistry & Photobiology, B: Biology 162 (2016) 199–207

Contents lists available at ScienceDirect

Journal of Photochemistry & Photobiology, B: Biology

journal homepage: www.elsevier.com/locate/jphotobiol

Biosynthesis of ZnO nanoparticles using *Jacaranda mimosifolia* flowers extract: Synergistic antibacterial activity and molecular simulated facet specific adsorption studies

Deepali Sharma [a,*], Myalowenkosi I. Sabela [a], Suvardhan Kanchi [a,*], Phumlane S. Mdluli [a], Gulshan Singh [b], Thor A. Stenström [b], Krishna Bisetty [a,*]

[a] Department of Chemistry, Durban University of Technology, P.O. Box 1334, Durban 4000, South Africa
[b] SARChi Chair, Institute for Water and Wastewater Technology, Durban University of Technology, P.O. Box 1334, Durban 4000, South Africa

ARTICLE INFO

Article history:
Received 18 May 2016
Received in revised form 22 June 2016
Accepted 23 June 2016
Available online 25 June 2016

Keywords:
Biosynthesis
Jacaranda mimosifolia flowers extract
Zinc oxide nanoparticles
Antibacterial activity

ABSTRACT

The naturally occurring biomolecules present in the plant extracts have been identified to play an active role in the single step formation of nanoparticles with varied morphologies and sizes which is greener and environmentally benign. In the present work, spherical zinc oxide nanoparticles (ZnO NPs) of 2–4 nm size were synthesized using aqueous extract of fallen *Jacaranda mimosifolia* flowers (JMFs), treated as waste. The microwave assisted synthesis was completed successfully within 5 min. Thereafter, phase identification, morphology and optical band gap of the synthesized ZnO NPs were done using X-ray diffraction (XRD), high resolution transmission electron microscopy (HRTEM) and UV–Visible spectroscopy techniques. The composition of JMFs extract was analyzed by gas chromatography–mass spectrometry (GC–MS) and the ZnO NPs confirmation was further explored with fourier transform infrared spectroscopy (FTIR). The GC–MS results confirmed the presence of oleic acid which has high propensity of acting as a reducing and capping agent. The UV–Visible data suggested an optical band gap of 4.03 eV for ZnO NPs indicating their small size due to quantum confinement. Further, facet specific adsorption of oleic acid on the surface of ZnO NPs was studied computationally to find out the impact of biomolecules in defining the shape and size of NPs. The viability of gram negative *Escherichia coli* and gram positive *Enterococcus faecium* bacteria was found to be 48% and 43%, respectively at high concentration of NPs.

1. Introduction

Nature acts as a "bio-laboratory" which provides ways and insight into the synthesis of advanced nanomaterials using a biomimetic approach. Synthesis of nanoparticles (NPs) with controlled size and morphology is a challenging part which is highly dependent on the design of the protocols. Different viable methodologies have been designed for the fabrication of NPs with unique size dependent properties. The concept of green chemistry and engineering has provided a guidance for the environmentally synthesis which are not harmful to environment and human health [1]. In the past few years, biotemplates from natural sources like microorganisms and plant extracts have been a source of inspiration for designing complex nanomaterials with high surface area and potent applications in commercial products, biosensors, catalysis, as well as environmental technologies [2]. The biological approach is alternative to the chemical methods being greener, energy saving and cost effective. Regarding the stability, the NPs are innoxious due to coating of biological molecules and hence, they are more biocompatible than the NPs prepared by chemical methods [3]. The biomolecules present in the extract of plants act as stabilizing agents in the formation of NPs [4,5].

Among different semiconductors and metal oxides, ZnO is one of the most promising materials because of its unique characteristics which are responsible for novel biological functionalities. In the nanostructure form it has become the focus of attention for research community due to its unique antifungal [6], antibacterial [7], antiviral [8], wound healing [9], UV filtering properties, high catalytic and photochemical activity, excellent stability, biocompatibility, environmental friendliness and low cost [10,11]. Therefore, it is crucial to devise tunable synthesis of ZnO NPs with desired morphology and size to further explore their unveiled potentials thereby enabling researchers to manipulate the present material for the fabrication of devices. The literature provides an insight into different approaches for the fabrication of ZnO nanostructures like gas phase methods which include chemical vapour deposition

* Corresponding authors.
E-mail addresses: dpschem@gmail.com (D. Sharma), ksuvardhan@gmail.com (S. Kanchi), bisettk@dut.ac.za (K. Bisetty).

http://dx.doi.org/10.1016/j.jphotobiol.2016.06.043
1011-1344/

(CVD), physical vapour transport (PVT) and pulsed layer deposition (PLD) [12]. Chemical methods have been found to be cost effective and alternative to gas phase methods. Mechanochemical [13,14], solvothermal [15,16], sol-gel [17,18], precipitation [19], hydrothermal [20,21] and microwave methods [22,23] have been classified under chemical methods. Among these, hydrothermal method is widely used due to green, low cost and low temperature synthesis. This method is modified with the use of capping or templating agents which aid in modifying the shape of NPs by adsorbing on the specific facet of a metal oxide crystal [24].

In the recent years, different types of plant extracts have been reported to be used as reducing or capping agents in the synthesis of NPs. Some of the examples include the eco-friendly synthesis of ZnO NPs using leaves extract of *Pongamia pinnata* [25], *Nerium oleander* [26], aloe leaf broth [27], *Solanum nigrum* [28], apple pectin [29] and aqueous extract of *Vitex negundo L.* [30]. The biomolecules present in the plant extracts act as efficient capping agents thereby playing a pivotal and versatile role in the NPs synthesis. The capping agents appear to stabilize NPs by different mechanisms that include electrostatic stabilization, steric stabilization, stabilization by hydration forces, depletion stabilization and stabilization using van der Waals forces. The stabilization of NPs is important for their functions and different applications [31].

Flowers are of great aesthetic value and maintain ecological balance in the environment. They are mainly utilized for their beauty as they radiate different colours to the surroundings. They serve the purpose when they bloom but when once wilt they fall off as trash. *Jacaranda mimosifolia* belongs to Bignoniaceae family and is widely grown in warm parts of the world. It has showy blue or violet flowers and has been found to have antiseptic and antibiotic qualities. Traditionally, the flowers, leaves and barks are used to ease neuralgia and varicose veins and also being scientifically proven to treat leukemia [32]. In the present work, the fallen flowers of *Jacaranda mimosifolia* plant normally regarded as waste were used for the biosynthesis of ZnO NPs for the first time to the best of our knowledge. ZnO nanostructures have been reported to be effective against the growth of bacteria [33]. Thus, the synthesized ZnO NPs were evaluated for the antibacterial activity against gram positive (*Enterococcus faecium*) and gram negative (*Escherichia coli*) bacteria. Generation of reactive oxygen species (ROS) mainly hydroxyl and superoxide radicals resulting in the oxidative stress is found to be the underlying mechanism for the bacterial cell death or static growth. The release of metal ions on interaction with the cellular components contributes to the bioactivity of the NPs [34]. To elucidate the contribution of oleic acid in the formation of ZnO NPs, its adsorption on different facets of ZnO was carried out computationally as the NP shape and size is dependent on the exposure of different facets of a crystal.

2. Experimental

2.1. Chemicals and Reagents

Zinc gluconate hydrate ($C_{12}H_{22}O_{14}Zn.xH_2O$, purity 97%), sodium hydroxide (NaOH, purity ≥98%) and methanol (CH_3OH, HPLC grade, ≥99.9%) were purchased from Alfa Aesar, Fluka and Sigma Aldrich, respectively. Phosphate buffered saline (PBS) tablets (pH 7.4) were acquired from Sigma Aldrich. Ultra-pure deionized water from PURITE (18 MΩ) system was used in all the experiments.

2.2. Synthesis of ZnO NPs Using the Extract of Jacaranda mimosifolia Flowers

The extract used in the synthesis of ZnO NPs was prepared by dissolving 1.0 g of dried and powdered *Jacaranda mimosifolia* flowers (collected in Durban, South Africa) in 100 mL deionized water and heating at a constant temperature of 90 °C for 1 h on a magnetic stirrer with a hot plate. The extract was filtered and used further in the synthesis. In a typical experiment, to 100 mL of zinc gluconate hydrate (0.1 M), 100 mL of *Jacaranda mimosifolia* flowers (JMFs) extract and 100 mL of NaOH (0.4 M) was added while stirring the mixture for 15 min. The mixture was then exposed to microwave irradiation for 5 min in a microwave oven (SAMSUNG ME9114W operating at 100% power of 1000 W and frequency of 2.45 GHz). The use of microwave irradiations offers homogenous heating, rapid and facile synthesis. The formation of ZnO NPs was indicated by the milky white precipitate powder which was filtered and subsequently washed with ethanol and deionized water. The final product was dried in an oven at a constant temperature of 60 °C for about 3 h. To know the effect of capping agent present in the extract, ZnO NPs were synthesized using 0.1 M zinc gluconate hydrate and 0.4 M NaOH without the use of extract keeping the reaction conditions same.

2.3. Materials Characterization

X-ray diffraction study was carried out using a Bruker AXS D8 diffractometer with CuKα radiation (λ = 1.5418 Å) at 40 kV over a 2θ range from 10° to 70° at a scanning rate of 0.05 min^{-1}. The size and morphology of the ZnO NPs was investigated by high resolution transmission electron microscope (HRTEM) model JEM 2100 (MAX OXFORD Instruments) equipped with a LaB_6 emitter. The samples were dispersed in distilled water and ultrasonicated for 30 min before analysis following the standard protocol. The absorption studies were carried out on a UV 2450 Spectrophotometer (Shimadzu, Japan) within the wavelength ranging from 200 to 800 nm. The colloidal solution of the sample was prepared by dissolving approximately 1.0 mg of ZnO nanopowder in 50 mL ultra-pure deionized water. FTIR spectra of ZnO NPs samples and extract of JMFs were recorded in the range of 4000–500 cm^{-1} on Varian 800 FTIR Scimitar Series supplied by SMM Instruments (Durban, SA).

To predict the composition of JMFs extract and predominent capping agent, GC–MS analysis of the methanolic extract was carried out. Accurately weighed 1.0 mg of the dried and powdered sample of JMFs was dissolved in methanol and stirred for 30 min followed by filtering through 0.45 μm nylon filter. Finnigan MAT GCQ system with splitless injector mode was employed for the sample analysis. The injector temperature was set at 250 °C and 200 °C for a ZB-5MS fused silica capillary column with dimensions 30 m × 0.25 mm × 1 μm. The carrier gas was helium with flow rate of 1 mL min^{-1} and the amount of sample injected was 1 μL. The MS conditions were as follows: full scan in EI mode (50 to 650 amu), transfer line temperature: 270 °C and ion source temperature: 200 °C. The compounds identified in JMFs extract sample were verified by comparing them to those within the NIST library.

2.4. Adsorption Studies Using Molecular Modeling

To understand the role of capping agents present in the JMFs extract, adsorption studies were carried out using adsorption locator and forcite modules in MATERIALS STUDIO 8.0 [35,36]. The capping agent i.e. oleic acid was sketched in Accelrys Materials Studio software package and geometrically optimized with COMPASS forcefield using forcite module to get the energy minimized structure. Three dimensional (3D) ZnO surfaces (101, 100 and 002) were built by importing the crystal structure of ZnO from the structure library of MATERIALS STUDIO 8.0. The oleic acid molecules were allowed to adsorb on each of the designed ZnO surface by setting up the task to *simulated annealing* with *fine* quality where *adsorbate* was oleic acid with different *loading* values. The COMPASS forcefield was assigned to charges of atoms with *Ewald & group based* summation method. The concentration profile of oleic acid molecules on the ZnO surface was obtained by running forcite calculation on the whole system (oleic acid molecules adsorbed on the surface of ZnO).

2.5. Bacteriological Toxicity Assessment by Standard Plate Count Method/ Colony Forming Units (CFU) Measurements

The viability of ZnO NPs treated and untreated *E. coli* cultures were determined by standard plate count method. The *Escherichia coli* ATCC 25922 and *Enterococcus faecium* ATCC 35667 cells were grown to O.D of 0.6 at 600 nm (35 ± 1 °C, 10^6 CFU mL^{-1}), pelletized by centrifugation (4000 ×*g* for 3 min at 4 °C), washed thrice by phosphate buffer saline (PBS, pH = 7.4) and finally suspended into PBS containing varying concentrations (10, 25, 50, 75, 100 μg mL^{-1}) of NPs synthesized using JMFs extract and without JMFs extract. Bacterial culture in Luria Bertani (LB) broth without NPs served as negative control. The cells were grown for 120 min at 35 ± 1 °C and were serially diluted in PBS at pH 7. The dilutions were plated on LB agar plates. After overnight incubation at 37 °C, the number of CFU was counted manually. All the experiments were conducted in triplicate.

3. Results and Discussion

ZnO NPs were formed via the simple method of alkali precipitation of zinc gluconate where the compounds present in the JMFs extract reduced the formed $Zn(OH)_2$ precursors. The schematic synthesis of ZnO NPs is shown in Fig. 1. The mechanism is explained on the basis that the biomolecules such as fatty acids, phenolic compounds, saponins, alkanoids, flavanoids present in the extract form complexing agents with the precursors which initially starts the process of nucleation forming reverse micelle and then further causing reduction and shaping of NPs [37–39]. The GC–MS results reveals that 1,6 dimethyldecahydro napthalene, oleic acid and citronellyl propionate are predominantly present in the JMFs extract. Based on the GC–MS, purity and fit values, oleic acid was selected as a reducing and capping agent for the synthesis of ZnO NPs. When zinc gluconate was dissolved in water, colourless solution was formed due to the presence of $[Zn(H_2O)_6]^{2+}$ ions. The addition of NaOH produces a white precipitate of ZnO NPs in the core of a micelle. The capping agent acts as a stabilizing agent by adhering onto the surface of NPs forming a protective layer and controlling the particle size [40].

The microwave irradiations act as an efficient, environment friendly and economical heating method for the synthesis of NPs while maximizing the yield. The household microwave ovens also lead to formation of metal and metal oxide NPs with good crystallinity and optical properties [41,42].

In the case of synthesis of NPs, the reaction rate and nucleation are dependent on the heating rate. The microwave heating is an alternative source for rapid volumetric heating with shorter reaction time, high reaction rate, selectivity and yield as compared to conventional heating methods. The enhancement in the reaction rate is caused predominantly by the rapid superheating of the solvent by microwaves. The solvent is also found to play an important role in the microwave-assisted synthesis. The more polar the solvent is higher is its ability to couple with microwave energy, leading to the rapid increase in temperature and fast reaction rate. The dielectric heating effect of microwaves is generated due to dipole moment interaction of the molecules and high frequency electromagnetic radiations. Since, water has a high dipole moment; it is a best solvent for the synthesis of NPs using microwaves [43]. As soon as aqueous solution containing zinc gluconate, extract and NaOH were exposed to microwave heating, the reaction completed within 5 min; there was enhancement in the reaction rate and nucleation which was indicated by the milky white precipitate powder leading to the formation of ZnO seeds.

The formation of NPs take place in two steps, nucleation and growth. When the supersaturation stage is achieved, the system enters the growth phase in which there is no formation of additional nuclei but existing clusters grow larger in size. Subsequently, nucleation and

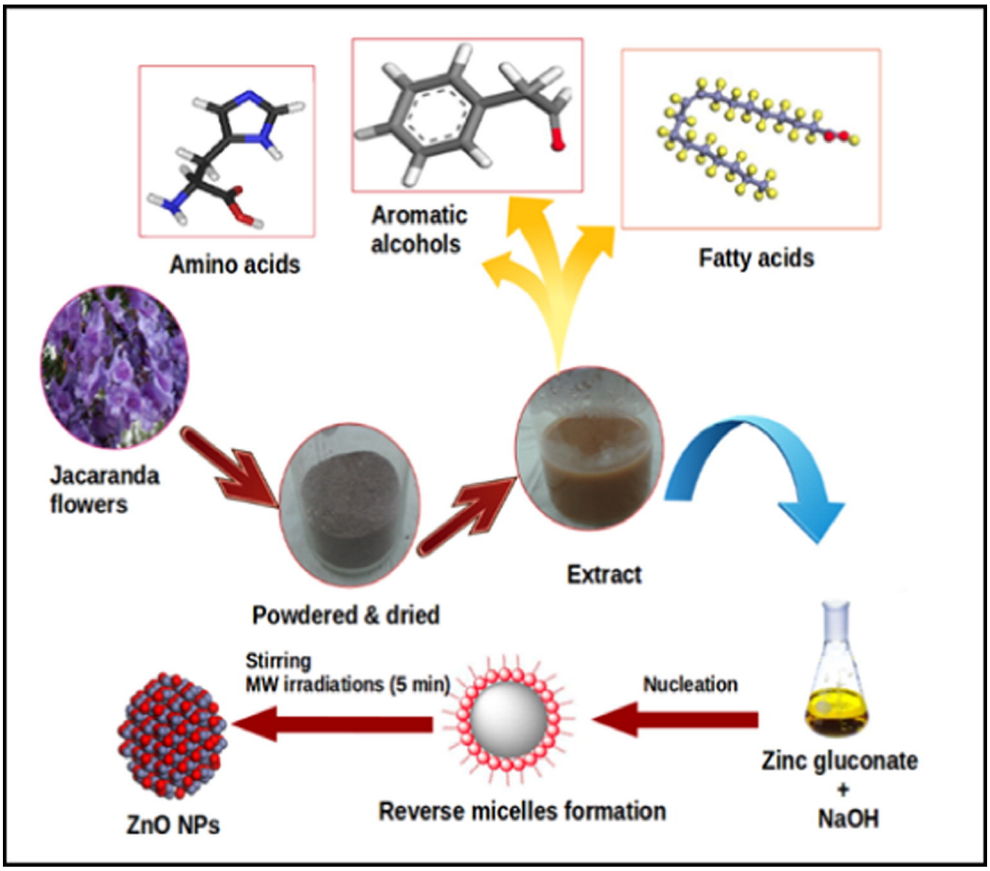

Fig. 1. Schematic representation of synthesis of ZnO NPs using JMFs extract.

growth are influenced by the heating rate, the microwave radiations leads to the formation of large amount of nuclei. Once the nucleation starts, the reaction system enters the growth process and nuclei with small sizes grow rapidly thereby shortening the overall process of formation of NPs. The extract used acts as a capping agent and use of microwave irradiations leads to formation of NPs with smaller size. These seeds assemble together as clusters due to their high surface energy which grow rapidly to form NP aggregates [44].

The XRD analysis of ZnO NPs synthesized using the JMFs extract exhibited typical diffraction peaks at 32.25° (100), 34.90° (002), 36.74° (101), 47.99° (102), 57.06° (110) and 63.31° (103) indexed to the crystalline ZnO wurtzite structure with P63mc space group whereas NPs formed without the use of JMFs extract exhibited peaks at 32.38° (100), 35.08° (002), 36.80° (101), 48.12° (102), 57.14° (110) and 63.42° (103), respectively [45] (Fig. 2). The lattice parameters for the hexagonal unit cell such as d-spacing (d), lattice constants (a, c) and unit cell volume (V) were calculated using the Lattice Geometry Equations [46] and also summarized in Table 1:

$$\frac{1}{d^2} = \frac{4}{3}\left(\frac{h^2 + hk + k^2}{a^2}\right) + \frac{l^2}{c^2} \quad (1)$$

$$V = \frac{\sqrt{3a^2c}}{2} \quad (2)$$

where, *h, k* and *l* are miller indices.

The calculated values of c/a ratio for ZnO NPs (Table 1) are close to ideal value of 1.633 for ZnO hexagonal cell. The deviation from the ideal wurtzite crystal is probably due to lattice stability and ionicity [47].

The morphology and size of the ZnO NPs was demonstrated by HRTEM images. Fig. 3A represents the ZnO NPs in the size range of 2–4 nm synthesized with JMFs extract whereas Fig. 3B shows the ZnO NPs with average diameter of 8–11 nm and spherical morphology prepared without the use of JMFs extract. The dark spots in the micrographs are the NPs clustered together due to their small size. The clear lattice fringe widths with the values of 0.24 nm and 0.26 nm in the HRTEM images (Fig. 3A and B) corresponds to 101 and 002 crystal planes and are indicative of the crystalline nature of ZnO NPs.

The semiconductor band structure of ZnO NPs has been characterized via UV–Visible absorption spectroscopy. Fig. 4 inset shows the UV–Visible spectra of ZnO NPs synthesized with and without JMFs extract showing absorption peaks at 265.91 nm and 278.9 nm, respectively. Therefore to better understand the role of capping agent in the JMFs extract, the optical band gap for the ZnO NPs was calculated using the

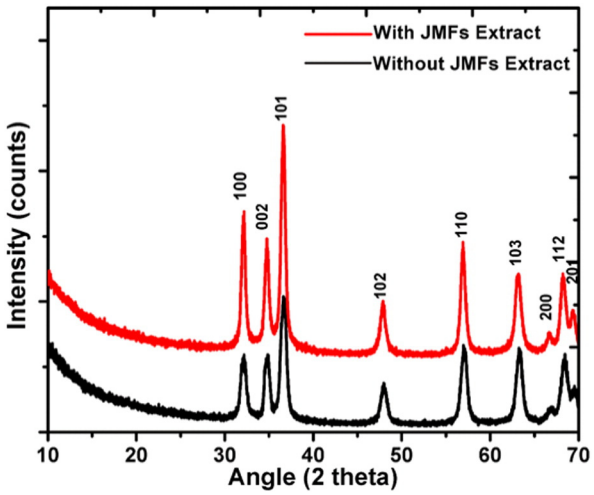

Fig. 2. XRD diffraction pattern of ZnO NPs with and without the use of JMFs extract.

Table 1
Lattice parameters of ZnO NPs synthesized using with and without JMFs extract.

Sample	2θ	hkl	d-spacing (Å)	LP (Å)	UCV (Å^3)
ZnO NPs (with extract)	32.25°	100	2.773	a = 3.205	45.73
	34.90°	002	2.568	c = 5.141	
	36.74°	101	2.443	c/a = 1.604	
ZnO NPs (without extract)	32.28°	100	2.770	a = 3.202	45.42
	35.08°	002	2.555	c = 5.116	
	36.80°	101	2.440	c/a = 1.598	

LP: Lattice parameters; UCV: Unit cell volume.

expression proposed by Tauc, Davis and Mott [48],

$$(h\nu\alpha) = A(h\nu - Eg)^n \quad (3)$$

where, h is Planck's constant, ν is frequency of vibration, α is absorption coefficient, Eg is band gap, A is proportionality constant and n denotes the nature of sample transition. The respective direct band gaps were found to be 4.07 eV and 3.74 eV for ZnO NPs synthesized with and without JMFs extract, probably due to quantum confinement (Fig. 4). With the decrease of the particle size, there is an increase in the energy gap of electronic transitions [49] i.e., as the system becomes more confined, the energy separation between adjacent levels increases and also discrete energy levels arises at the band edges [50].

The FTIR was employed to further probe the role of biomolecules present in the JMFs extract for the formation of ZnO NPs. As shown in Fig. 5, the FTIR spectrum of JMFs extract exhibits broad peak at 3373.12 cm^{-1} corresponding to O—H stretching vibration whereas the peaks at 2942.29 cm^{-1}, 2830.04 cm^{-1}, 1647.43 cm^{-1} and 1031.62 cm^{-1} correspond to C—H stretching, carbonyl group (C═O) and C—H bending, respectively. The peaks related to the following functional groups in the extract indicate the existence of different biomolecules; the major being oleic acid which was further confirmed through GC–MS analysis. The spectra of ZnO NPs synthesized with and without JMFs extract shows characteristic peaks of Zn—O stretching at 745.54 cm^{-1} and 779.45 cm^{-1}, respectively confirming the formation of ZnO NPs [51]. There was also a significant disappearance of peaks corresponding to that of extract in the spectra of ZnO NPs. The weak peak around 1445.85 cm^{-1} was broadened as seen in the spectra of NPs which could be attributed to C—H bending in methanol since the samples were prepared in methanol.

From the literature reports on the synthesis of metal oxide NPs with plant extract [52–54], it is evident that biomolecules play a pivotal role in the reduction of metal oxide salts and stabilization of NPs, but very few identify the biomolecules involved in the process of formation of NPs. In this regard, GC–MS analysis of methanolic extract of JMFs was carried out to identify the biomolecules present in the extract and to understand their impact on the morphology and size of NPs. Fig. 6 illustrates the GC–MS chromatogram of the methanolic extract of the JMFs where different components were identified. In the retention time ranging from 15:03 to 20:03 min where the high intensity peaks were present, the elution order was 1, 6 dimethyldecahydronapthalene, oleic acid and citronellyl propionate. On the basis of purity fit, oleic acid was found to be the most significant capping agent molecule. Therefore, facet-specific binding adsorption studies were carried out to comprehend its role as a capping agent which has been explained in the subsequent section.

3.1. Adsorption of Oleic Acid on the Surface of ZnO NPs

Apart from many studies which focus on the quantum confinement effect of quantum dots such as ZnO NPs, the surface chemistry is very significant in order to understand the physical and chemical properties of NPs. Consequently, the selective interaction of ZnO NPs with capping agents such as oleic acid is critically vital to enhance biocompatibility and viability, making these nanomaterials a suitable candidate in applications involving biological studies. In this paper, we therefore,

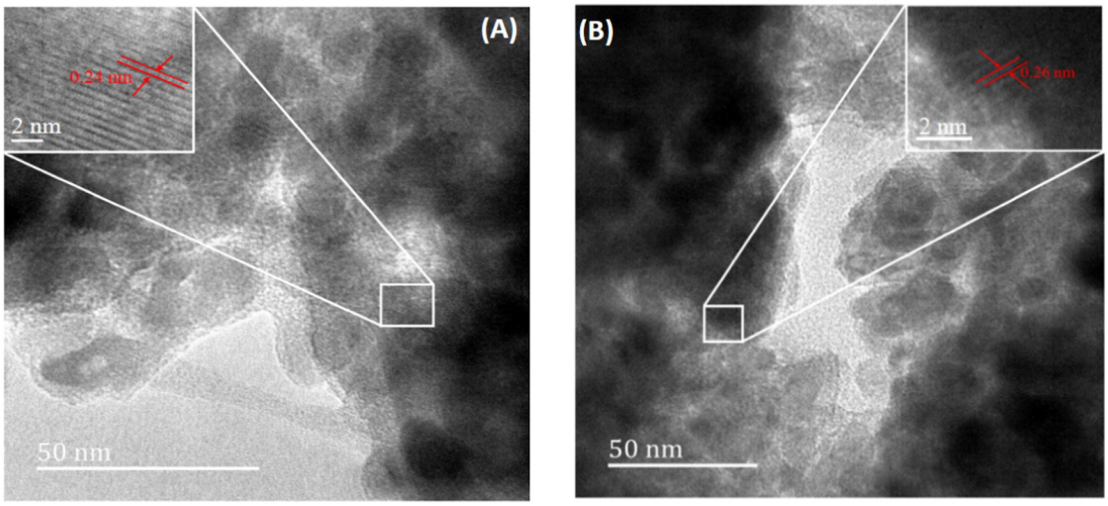

Fig. 3. HRTEM micrographs of ZnO NPs (**A**) with JMFs extract; (B) without JMFs extract.

employed molecular dynamics to demonstrate that physical and chemical properties of ZnO nanocrystal is induced by surface chemistry which preferably lead to isotropic and anisotropic nanomaterials. The role of capping agent in defining the size and shape was studied by simulating three crystal lattice parameters as shown in Fig. 7. It was demonstrated that ZnO NPs have varied shape evolution and potentially different facets which lead to facet-driven growth of ZnO to different shapes, thereby fine-tuning their optical properties. For many studies, facets such as (111) and (101) are highly studied because of their potential to drive preferential growth of nanomaterial which is the main contributor of their varied optical properties [55]. In order to simulate the variation of the reaction parameters, three facets, (002), (100) and (101), were studied. It was demonstrated that as the concentration of oleic acid was increased, the strength of adsorption favoured the (101) facet. The preferential passivation of (101) facet was evident from concentration profile shown in Fig. 8C. In these Fig. 8(A, B and C), it can be seen that the average distance of oleic acid on the surface of ZnO cluster were located within the distance of an average of 1.4 Å as compared to other facets on which the oleic molecules were located on the varying distance of 4 and 9 Å for (100) and (002) facets, respectively. These results confirmed previous study which indicated that the presence of oleic acid could drive the preferential growth of zinc oxide nanomaterials to nanorods array and other structures [56].

The most favoured model from Fig. 7 was obtained by further calculating the interaction energy of each model. The interaction ($E_{interaction}$) was calculated as follows:

$$E_{interaction} = E_{complex} - (E_{ligand} + E_{surface}) \quad (4)$$

$E_{complex}$ is the energy of the surface and oleic acid, E_{ligand} is the energy of the oleic acid and $E_{surface}$ is the energy of the surface (ZnO-100, ZnO-002 and ZnO-101) without ligands. The negative $E_{interaction}$ values indicate an attractive or strong oleic acid to ZnO interactions. The interaction energies of models depicted in Fig. 7 were calculated using Eq. (4) as presented in Table 2.

The interaction energies in Table 2 reveals the trend, ZnO-101 > ZnO-002 > ZnO-100. The high interaction for ZnO-101 symbolizes that oleic acid binds stronger on ZnO-101 surface than the other surfaces. Although, the interaction gives the general picture of the interaction of oleic acid with ZnO surface, this trend does not eliminate the fact that all surfaces can potentially interact with oleic acid but to the lesser extent than the 101-surface. This is merely an indication that more oleic

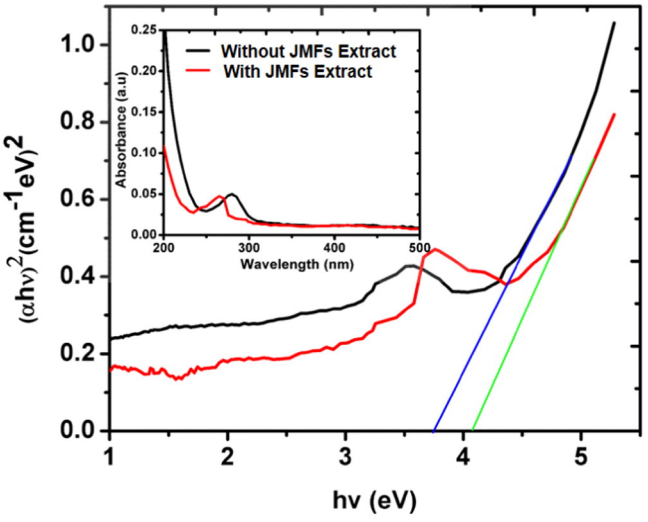

Fig. 4. Tauc Plot of ZnO NPs with and without use of JMFs extract showing inset of UV–Vis spectra.

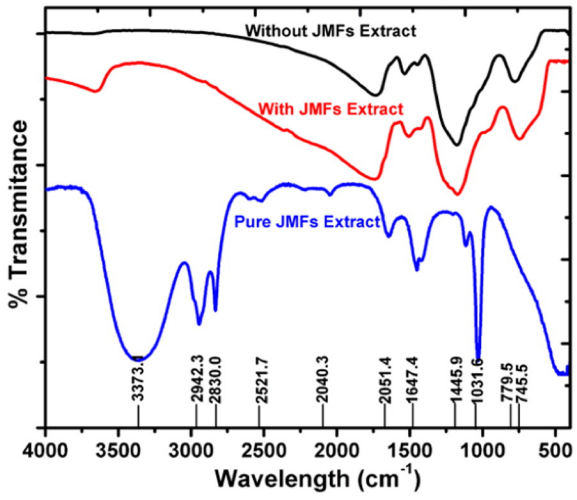

Fig. 5. FTIR spectra of methanolic pure JMFs extract , ZnO NPs synthesized with and without the use of extract.

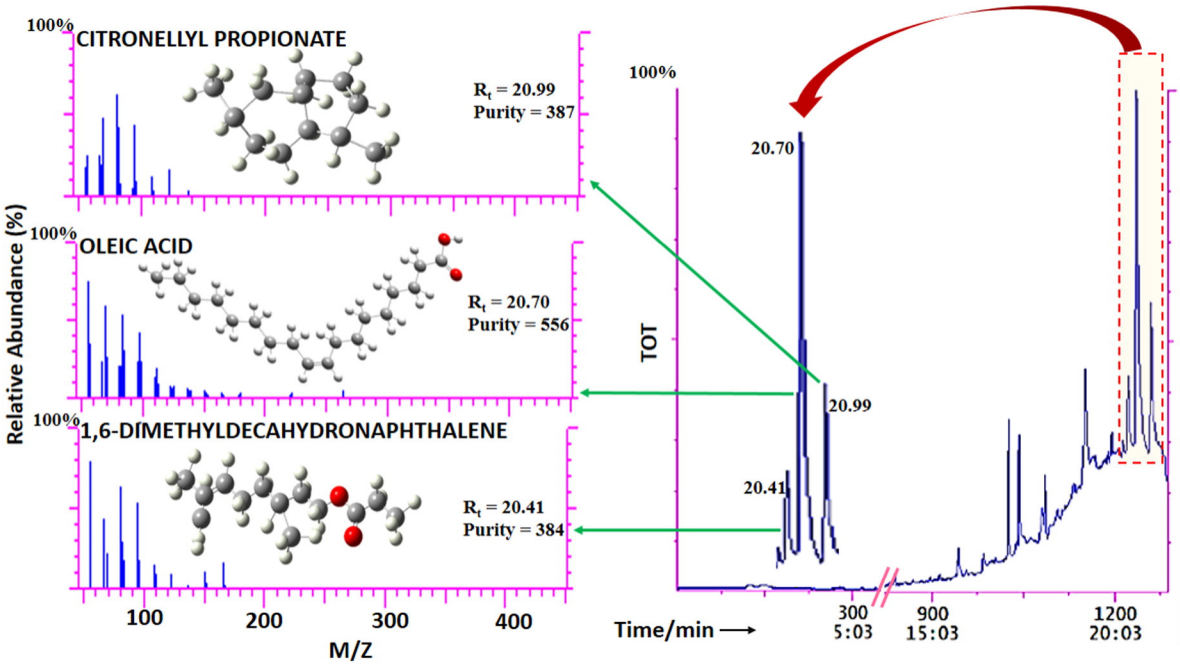

Fig. 6. GC–MS chromatogram of methanolic extract of JMFs.

acid molecules shall interact with 101 surfaces leaving the other surfaces (ZnO-002 and ZnO-100) with less number of oleic acid molecules. The concentration profiles of different facets of ZnO shown in Fig. 8A, B and C are good indicators to probe the vicinity of functional groups on the surface of metal oxide. The concentration profile proved that the affinity of the oleic acid is more pronounced on 101 facet, which are situated closer to the surface by about 1.4 Å. This selective adsorption was reported elsewhere to drive the rapid growth of ZnO NPs to pencil-like nanorods [57].

3.2. Antibacterial Activity of Synthesized ZnO NPs

Antibacterial property of ZnO NPs was analyzed by treating bacterial culture (gram negative and gram positive) with varying concentration

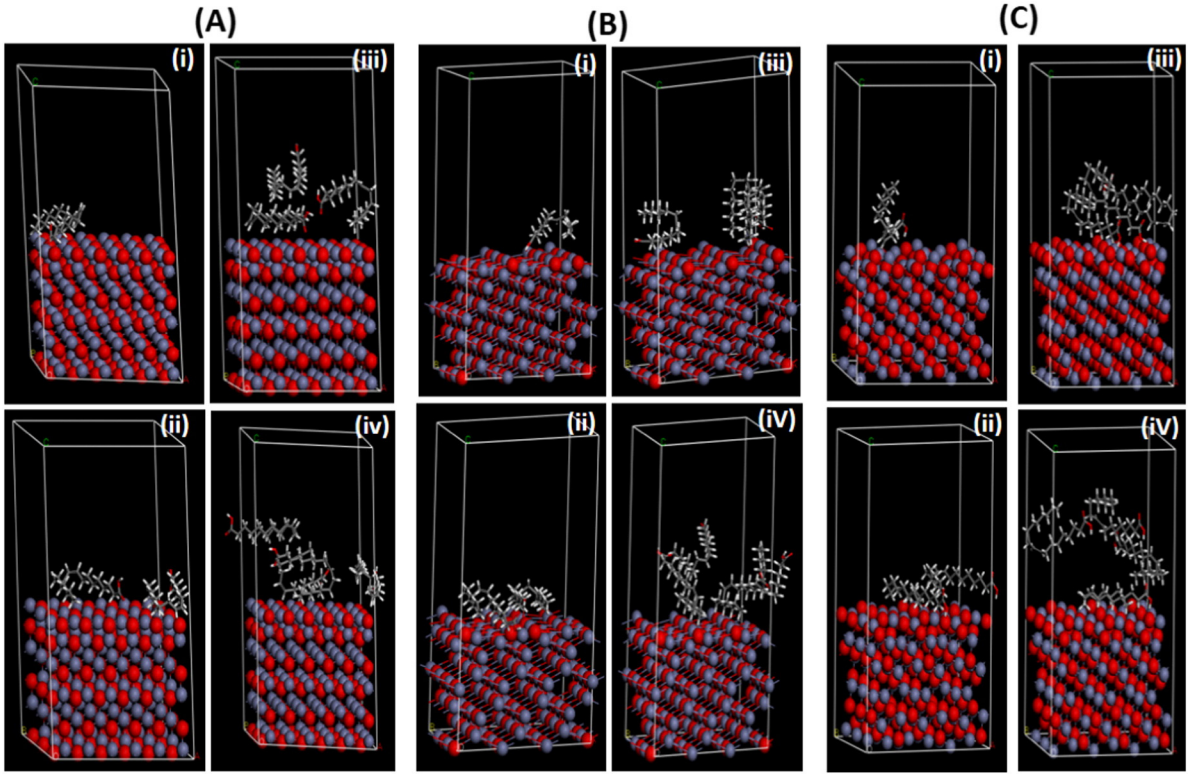

Fig. 7. Adsorption of oleic acid molecules onto different surfaces (A) 002 (B) 100 and (C) 101 of ZnO clusters.

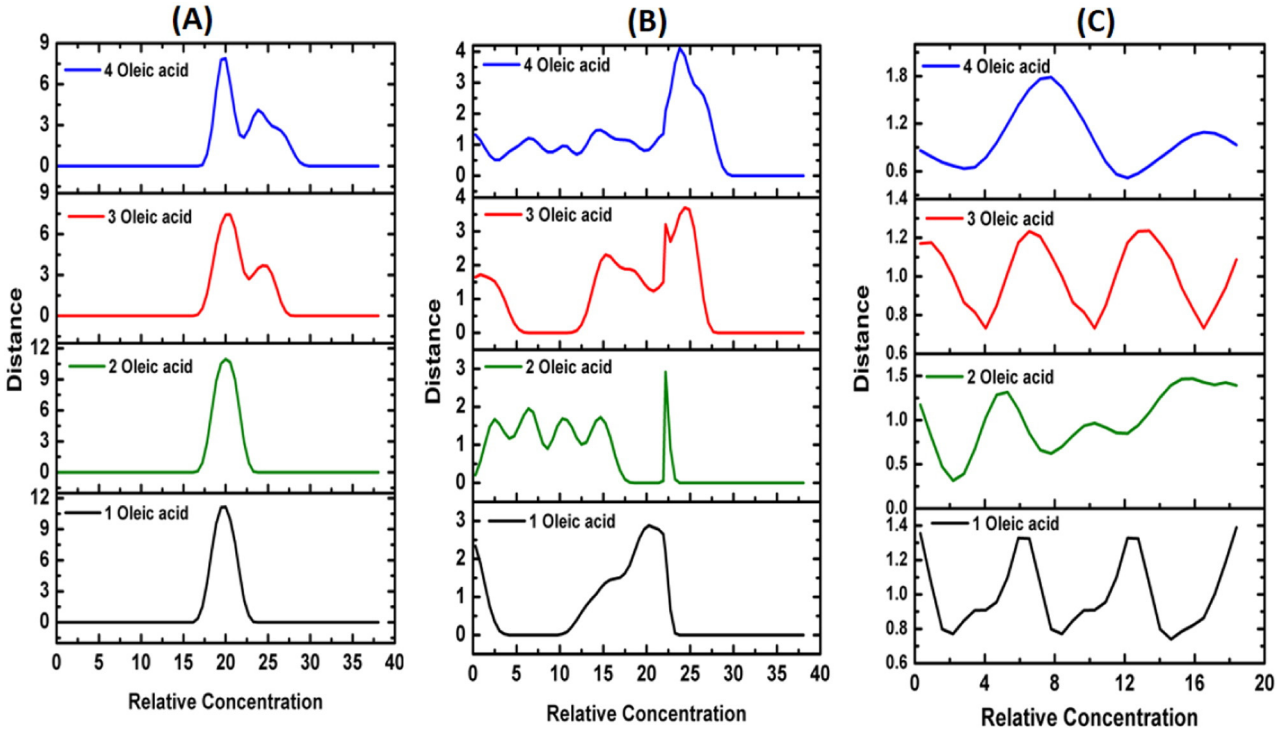

Fig. 8. Concentration profile of oleic acid molecules adsorbed on (A) 002 (B) 100 (C) 101 facets of ZnO.

of NPs (10–100 μg mL^{-1}) and viability was assessed by standard plate count method. It was observed that as the concentration of ZnO NPs increased, colony forming units (CFU) count of gram negative (*Escherichia coli*) and gram positive (*Enterococcus faecium*) bacterial cultures decreased in the standard plate count method. ZnO NPs prepared using JMFs extract and without JMFs extract exhibited antibacterial property as evident from the present results (Fig. 9A–B). The viability of *E.coli* and *E. faecium* was assessed in the presence of different concentrations of NPs (10–100 μg mL^{-1}). The percent viability of the ZnO NPs exhibited stronger antibacterial activity against gram positive *E. faecium* than against gram negative *E. coli.* The results reported were in concurrence with previously published reports showing the antibacterial activity of ZnO NPs [58]. The important reason could be the difference in the cell wall structure of gram positive and gram negative bacteria. The cell wall of gram positive bacteria is normally composed of peptidoglycan which forms 80% of the cell wall. The remaining 10–20% of the cell wall is composed of teichoic acids, other proteins and lipopolysaccharides which is outer membrane. In the case of gram negative bacteria, peptidoglycan forms 10% of the cell wall but the outer membrane is composed of 50% lipopolysaccharides, 35% phospholipids and 15% lipoproteins. Thus, outer membrane in gram negative bacteria is tightly packed, hence, providing protection and sensitivity to antibacterial agents [59]. Moreover, the antibacterial activity depends on the size of NPs and also infectivity and sensitivity of different strains vary [60]. Therefore, ZnO NPs synthesized using the extract of JMFs were in the range of 2–4 nm size as compared to NPs fabricated in the absence of JMFs extract (8–11 nm) and the *E. faecium* ATCC 35667 strain has been reported to be more pathogenic than *E. coli* ATCC 25922.

Table 2
Adsorption energy of oleic acid molecules on the facets of ZnO nanocluster.

Facet	Adsorption energy (kcal/mol) of number of oleic acid molecules			
	1	2	3	4
100	−31.242	−65.724	−97.977	−121.28
002	−45.668	−92.127	−135.95	−167.62
101	−64.297	−128.69	−178.6	−221.92

E.coli and *E. faecium* when treated with 100 μg mL^{-1} concentration of ZnO NPs synthesized without extract were found to be 59% and 51% viable (Fig. 9B) whereas the percent viability was 48% and 43%, respectively for the NPs synthesized using JMFs extract (Fig. 9A). The results indicated that the antimicrobial property of JMFs extract mediated synthesized ZnO NPs was higher than that of the NPs synthesized without JMFs extract at higher concentrations (Fig. 9A–B).

Furthermore, there was statistically significant difference in cell viability at 100 μg mL^{-1} in *E.coli* and *E. faecium* when treated with ZnO NPs using extract ($p = 0.0448$). Similar trend was observed for concentrations 75, 50, and 25 μg mL^{-1} of NPs.

4. Conclusions

The results presented in the present work demonstrate the biosynthesis of ZnO NPs with a narrow size range of 2–4 nm using the extract of JMFs. The major finding was the presence of oleic acid as a capping agent in the synthesis of ZnO NPs, identified by GC–MS and FTIR. The peaks corresponding to the oleic acid and ZnO NPs were well depicted in the FTIR spectra as well. The capping agent, oelic acid was found to stabilize the resulting NPs. Furthermore, the other identified molecules like 1,6 dimethyldecahydronapthalene and citronellyl propionate could also function as capping agents. The second major finding is the facet specific binding of the oleic acid molecule on to the different surfaces of the ZnO. It was established on the basis of interaction energy and concentration profile that oleic acid preferred to adsorb on to (101) facet of ZnO as compared to the other (002) and (100) facets. This would lead to the understanding of the selective adsorption of molecules on to the surface of different NPs thereby driving into the formation with varied shapes and sizes.

The oleic acid stabilized ZnO NPs showed fairly good antibacterial activity against both gram negative *E. coli* and gram positive *E. faecium* bacteria. The antibacterial activity was pronounced in the case of gram positive bacteria (*E. faecium*) as the NPs could penetrate easily through the outer membrane due to the less compact nature as compared to that of gram negative bacteria. The synthesis reported here is reproducible in

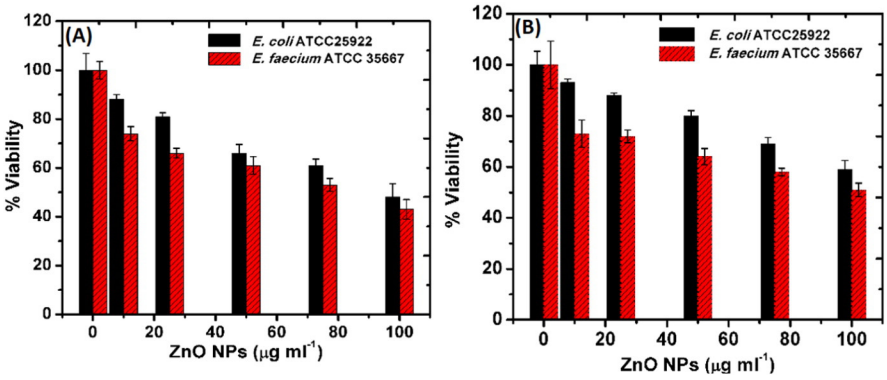

Fig. 9. Viability of bacteria in the presence of ZnO NPs synthesized using (**A**) JMFs extract, (B) without JMFs extract.

short time, cost effective and environmentally safe as it makes use of extract from the fallen waste JMFs for the first time.

Acknowledgements

Our grateful acknowledgement goes to Mr. S. R. Chetty for the GC–MS analysis; Durban University of Technology and National Research Foundation of South Africa for the financial support. We also thank the Centre for High Performance (CHPC), Cape Town, South Africa for the access to the Accelrys MATERIALS STUDIO 8.0 license and national cluster system.

References

[1] J.M. Patete, X. Peng, C. Koenigsmann, Y. Xu, B. Karn, S.S. Wong, Viable methodologies for the synthesis of high-quality nanostructures, Green Chem. 13 (2011) 482–519.
[2] M. Francavilla, A. Pineda, A.A. Romero, J.C. Colmenares, C. Vargas, M. Monteleone, R. Luque, Efficient and simple reactive milling preparation of photocatalytically active porous ZnO nanostructures using biomass derived polysaccharides, Green Chem. 16 (2014) 2876–2885.
[3] R. Selvakumar, N. Seethalakshmi, P. Thavamani, R. Naidu, M. Megharaj, Recent advances in the synthesis of inorganic nano/microstructures using microbial biotemplates and their applications, RSC Adv. 4 (2014) 52156–52169.
[4] R.M. Tripathi, A.S. Bhadwal, R.K. Gupta, P. Singh, A. Shrivastav, B.R. Shrivastav, ZnO nanoflowers: novel biogenic synthesis and enhanced photocatalytic activity, J. Photochem. Photobiol. B 141 (2014) 288–295.
[5] S. Ahmed, S. Annu, S. Ikram, S. Yudha, Biosynthesis of gold nanoparticles: a green approach, J. Photochem. Photobiol. B 161 (2016) 141–153.
[6] D. Sharma, J. Rajput, B.S. Kaith, M. Kaur, S. Sharma, Synthesis of ZnO nanoparticles and study of their antibacterial and antifungal properties, Thin Solid Films 519 (2010) 1224–1229.
[7] V. Lakshmi Prasanna, R. Vijayaraghavan, Insight into the mechanism of antibacterial activity of ZnO: surface defects mediated reactive oxygen species even in the dark, Langmuir 31 (2015) 9155–9162.
[8] T. Antoine, Y.K. Mishra, J. Trigilio, V. Tiwari, R. Adelung, D. Shukla, Prophylactic, therapeutic and neutralizing effects of zinc oxide tetrapod structures against herpes simplex virus type-2 infection, Antivir. Res. 96 (2012) 363–375.
[9] A.K. Barui, V. Veeriah, S. Mukherjee, J. Manna, A.K. Patel, S. Patra, K. Pal, S. Murali, R.K. Rana, S. Chatterjee, C.R. Patra, Zinc oxide nanoflowers make new blood vessels, Nanoscale 4 (2012) 7861–7869.
[10] C. Tamuly, I. Saikia, M. Hazarika, M. Bordoloi, N. Hussain, M.R. Das, K. Deka, Bio-derived ZnO nanoflower: a highly efficient catalyst for the synthesis of chalcone derivatives, RSC Adv. 5 (2015) 8604–8608.
[11] X. Sun, Q. Li, J. Jiang, Y. Mao, Morphology-tunable synthesis of ZnO nanoforest and its photoelectrochemical performance, Nanoscale 6 (2014) 8769–8780.
[12] B. Andrey, B. Arne, W. Alexander, W. Andreas, Fabrication of ZnO Nanostructures, Zinc Oxide Nanostructures, Pan Stanford Publishing, 2014 1–42.
[13] S. Liming, B. Ningzhong, Y. Kazumichi, D. Kazunari, G. Arunava, A.G. Craig, Direct synthesis of ZnO nanoparticles by a solution-free mechanochemical reaction, Nanotechnology 17 (2006) 5117.
[14] J. Lu, K.M. Ng, S. Yang, Efficient, one-step mechanochemical process for the synthesis of ZnO nanoparticles, Ind. Eng. Chem. Res. 47 (2008) 1095–1101.
[15] X. Bai, L. Li, H. Liu, L. Tan, T. Liu, X. Meng, Solvothermal synthesis of ZnO nanoparticles and anti-infection application in vivo, ACS Appl. Mater. Interfaces 7 (2015) 1308–1317.
[16] T. Ghoshal, S. Biswas, M. Paul, S.K. De, Synthesis of ZnO nanoparticles by solvothermal method and their ammonia sensing properties, J. Nanosci. Nanotechnol. 9 (2009) 5973–5980.
[17] M. Lima, D. Fernandes, M. Silva, M. Baesso, A. Neto, G. de Morais, C. Nakamura, A. de Oliveira Caleare, A. Hechenleitner, E. Pineda, Co-doped ZnO nanoparticles synthesized by an adapted sol–gel method: effects on the structural, optical, photocatalytic and antibacterial properties, J. Sol-Gel Sci. Technol. 72 (2014) 301–309.
[18] Y.L. Zhang, Y. Yang, J.H. Zhao, R.Q. Tan, P. Cui, W.J. Song, Preparation of ZnO nanoparticles by a surfactant-assisted complex sol–gel method using zinc nitrate, J. Sol-Gel Sci. Technol. 51 (2009) 198–203.
[19] Y. Wang, C. Zhang, S. Bi, G. Luo, Preparation of ZnO nanoparticles using the direct precipitation method in a membrane dispersion micro-structured reactor, Powder Technol. 202 (2010) 130–136.
[20] D. Ramimoghadam, M.Z. Bin Hussein, Y.H. Taufiq-Yap, Hydrothermal synthesis of zinc oxide nanoparticles using rice as soft biotemplate, Chem. Cent. J. 7 (2013) 136.
[21] M. Søndergaard, E.D. Bøjesen, M. Christensen, B.B. Iversen, Size and morphology dependence of ZnO nanoparticles synthesized by a fast continuous flow hydrothermal method, Cryst. Growth Des. 11 (2011) 4027–4033.
[22] D. Sharma, S. Sharma, B.S. Kaith, J. Rajput, M. Kaur, Synthesis of ZnO nanoparticles using surfactant free in-air and microwave method, Appl. Surf. Sci. 257 (2011) 9661–9672.
[23] I. Bilecka, P. Elser, M. Niederberger, Kinetic and thermodynamic aspects in the microwave-assisted synthesis of ZnO nanoparticles in benzyl alcohol, ACS Nano 3 (2009) 467–477.
[24] S.K. Ramakrishnan, M. Martin, T. Cloitre, L. Firlej, C. Gergely, Design rules for metal binding biomolecules: understanding of amino acid adsorption on platinum crystallographic facets from density functional calculations, Phys. Chem. Chem. Phys. 17 (2015) 4193–4198.
[25] M. Sundrarajan, S. Ambika, K. Bharathi, Plant-extract mediated synthesis of ZnO nanoparticles using *Pongamia pinnata* and their activity against pathogenic bacteria, Adv. Powder Technol. 26 (2015) 1294–1299.
[26] T.R. Lakshmeesha, M.K. Sateesh, B.D. Prasad, S.C. Sharma, D. Kavyashree, M. Chandrasekhar, H. Nagabhushana, Reactivity of crystalline ZnO superstructures against fungi and bacterial pathogens: synthesized using *Nerium oleander* leaf extract, Cryst. Growth Des. 14 (2014) 4068–4079.
[27] S. Gunalan, R. Sivaraj, V. Rajendran, Green synthesized ZnO nanoparticles against bacterial and fungal pathogens, Prog. Nat. Sci.: Mater. Int. 22 (2012) 693–700.
[28] M. Ramesh, M. Anbuvannan, G. Viruthagiri, Green synthesis of ZnO nanoparticles using *Solanum nigrum* leaf extract and their antibacterial activity, Spectrochim. Acta A Mol. Biomol. Spectrosc. 136 (Pt B) (2015) 864–870.
[29] A.-J. Wang, Q.-C. Liao, J.-J. Feng, P.-P. Zhang, A.-Q. Li, J.-J. Wang, Apple pectin-mediated green synthesis of hollow double-caged peanut-like ZnO hierarchical superstructures and photocatalytic applications, Cryst. Eng. Comm. 14 (2012) 256–263.
[30] S. Ambika, M. Sundrarajan, Green biosynthesis of ZnO nanoparticles using *Vitex negundo* L. extract: Spectroscopic investigation of interaction between ZnO nanoparticles and human serum albumin, J. Photochem. Photobiol. B 149 (2015) 143–148.
[31] B. Ajitha, Y.A. Kumar Reddy, P.S. Reddy, H.-J. Jeon, C.W. Ahn, Role of capping agents in controlling silver nanoparticles size, antibacterial activity and potential application as optical hydrogen peroxide sensor, RSC Adv. 6 (2016) 36171–36179.
[32] J. Joselin, T.S.S. Brintha, A.R. Florence, S. Jeeva, Phytochemical evaluation of Bignoniaceae flowers, J. Chem. Pharm. Res. 5 (2013) 106–111.
[33] K. Akhil, J. Jayakumar, G. Gayathri, S.S. Khan, Effect of various capping agents on photocatalytic, antibacterial and antibiofilm activities of ZnO nanoparticles, J. Photochem. Photobiol. B 160 (2016) 32–42.
[34] W. He, H.-K. Kim, W.G. Wamer, D. Melka, J.H. Callahan, J.-J. Yin, Photogenerated charge carriers and reactive oxygen species in ZnO/Au hybrid nanostructures with enhanced photocatalytic and antibacterial activity, J. Am. Chem. Soc. 136 (2014) 750–757.
[35] S. Kirkpatrick, C.D. Gelatt, M.P. Vecchi, Optimization by simulated annealing, Science 220 (1983) 671–680.
[36] S.W. Bunte, H. Sun, Molecular modeling of energetic materials: the parameterization and validation of nitrate esters in the COMPASS force field, J. Phys. Chem. B 104 (2000) 2477–2489.
[37] D. Sharma, S. Kanchi, K. Bisetty, Biogenic Synthesis of Nanoparticles: A Review, Arabian J, Chem, 2015.

[38] W.J. Crookes-Goodson, J.M. Slocik, R.R. Naik, Bio-directed synthesis and assembly of nanomaterials, Chem. Soc. Rev. 37 (2008) 2403–2412.
[39] A.K. Gade, P. Bonde, A.P. Ingle, P.D. Marcato, N. Durán, M.K. Rai, Exploitation of aspergillus Niger for synthesis of silver nanoparticles, J. Biobased Mater. Bioenergy 2 (2008) 243–247.
[40] H. Kumar, R. Rani, Structural and optical characterization of ZnO nanoparticles synthesized by microemulsion route, Int. Lett. Chem. Phys. Astron. 14 (2013) 26.
[41] A. Bhattacharjee, M. Ahmaruzzaman, T. Sinha, Surfactant effects on the synthesis of durable tin-oxide nanoparticles and its exploitation as a recyclable catalyst for the elimination of toxic dye: a green and efficient approach for wastewater treatment, RSC Adv. 4 (2014) 51418–51429.
[42] M.A. Bhosale, D.R. Chenna, J.P. Ahire, B.M. Bhanage, Morphological study of microwave-assisted facile synthesis of gold nanoflowers/nanoparticles in aqueous medium and their catalytic application for reduction of *p*-nitrophenol to *p*-aminophenol, RSC Adv. 5 (2015) 52817–52823.
[43] B. Baruwati, V. Polshettiwar, R.S. Varma, Chapter 7 Microwave-assisted synthesis of nanomaterials in aqueous media, aqueous microwave assisted chemistry, The Royal Society of Chemistry, 2010 176–216.
[44] X. Wang, J. Tian, C. Fei, L. Lv, Y. Wang, G. Cao, Rapid construction of TiO_2 aggregates using microwave assisted synthesis and its application for dye-sensitized solar cells, RSC Adv. 5 (2015) 8622–8629.
[45] K. Yoshio, A. Onodera, H. Satoh, N. Sakagami, H. Yamashita, Crystal structure of ZnO: Li at 293 K and 19 K by X-ray diffraction, Ferroelectrics 264 (2001) 133–138.
[46] C. Suryanarayana, M.G. Norton, Crystal structure determination. II: hexagonal structures, in: C. Suryanarayana, M.G. Norton (Eds.), X-Ray Diffraction: A Practical Approach, Springer US, Boston, MA 1998, pp. 125–152.
[47] H. Morkoç, Ü. Özgür, General Properties of ZnO, Wiley-VCH Verlag GmbH & Co. KGaA, Zinc Oxide, 2009 (pp. 1-76).
[48] J. Tauc, A. Menth, States in the gap, J. Non-Cryst. Solids 8–10 (1972) 569–585.
[49] L. Spanhel, Colloidal ZnO nanostructures and functional coatings: a survey, J. Sol-Gel Sci. Technol. 39 (2006) 7–24.
[50] R. Koole, E. Groeneveld, D. Vanmaekelbergh, A. Meijerink, C. Mello Donegá, Size effects on semiconductor nanoparticles, in: C. de Mello Donegá (Ed.), Nanoparticles: Workhorses of Nanoscience, Springer, Berlin Heidelberg, Berlin, Heidelberg 2014, pp. 13–51.
[51] V. Musat, A. Tabacaru, B.S. Vasile, V.-A. Surdu, Size-dependent photoluminescence of zinc oxide quantum dots through organosilane functionalization, RSC Adv. 4 (2014) 63128–63136.
[52] P. Rajiv, S. Rajeshwari, R. Venckatesh, Bio-fabrication of zinc oxide nanoparticles using leaf extract of *Parthenium hysterophorus* L. and its size-dependent antifungal activity against plant fungal pathogens, Spectrochim. Acta A Mol. Biomol. Spectrosc. 112 (2013) 384–387.
[53] M. Nasrollahzadeh, M. Maham, A. Rostami-Vartooni, M. Bagherzadeh, S.M. Sajadi, Barberry fruit extract assisted in situ green synthesis of Cu nanoparticles supported on a reduced graphene oxide-Fe_3O_4 nanocomposite as a magnetically separable and reusable catalyst for the *o*-arylation of phenols with aryl halides under ligand-free conditions, RSC Adv. 5 (2015) 64769–64780.
[54] M. Atarod, M. Nasrollahzadeh, S.M. Sajadi, Green synthesis of a Cu/reduced graphene oxide/Fe_3O_4 nanocomposite using Euphorbia wallichii leaf extract and its application as a recyclable and heterogeneous catalyst for the reduction of 4-nitrophenol and rhodamine B, RSC Adv. 5 (2015) 91532–91543.
[55] J. Chang, E.R. Waclawik, Colloidal semiconductor nanocrystals: controlled synthesis and surface chemistry in organic media, RSC Adv. 4 (2014) 23505–23527.
[56] A. McLaren, T. Valdes-Solis, G. Li, S.C. Tsang, Shape and size effects of ZnO nanocrystals on photocatalytic activity, J. Am. Chem. Soc. 131 (2009) 12540–12541.
[57] H. Wang, Y. Lian, A mechanistic study of oleic acid-mediated solvothermal shape controllable preparation of zinc oxide nanostructures, J. Alloys Compd. 594 (2014) 141–147.
[58] B. Pang, J. Yan, L. Yao, H. Liu, J. Guan, H. Wang, H. Liu, Preparation and characterization of antibacterial paper coated with sodium lignosulfonate stabilized ZnO nanoparticles, RSC Adv. 6 (2016) 9753–9759.
[59] X. Li, Y. Xing, Y. Jiang, Y. Ding, W. Li, Antimicrobial activities of ZnO powder-coated PVC film to inactivate food pathogens, Int. J. Food Sci. Technol. 44 (2009) 2161–2168.
[60] K.R. Raghupathi, R.T. Koodali, A.C. Manna, Size-dependent bacterial growth inhibition and mechanism of antibacterial activity of zinc oxide nanoparticles, Langmuir 27 (2011) 4020–4028.